Available online at www.sciencedirect.com
SCIENCE DIRECT®
Journal of Nuclear Materials 352 (2006) 136–143
journal of nuclear materials
www.elsevier.com/locate/jnucmat

A study of xenon aggregates in uranium dioxide using X-ray absorption spectroscopy

P. Garcia [a,*], P. Martin [a], G. Carlot [a], E. Castelier [a], M. Ripert [a], C. Sabathier [a], C. Valot [a], F. D'Acapito [b], J-L. Hazemann [c], O. Proux [d], V. Nassif [e]

[a] Centre d'Études de Cadarache, DEN/DEC/SESC/LLCC, Bâtiment 151, 13108 Saint-Paul-lez-Durance, cedex, France
[b] GILDA/CRG-ESRF 6 rue Jules Horowitz, B.P. 220, 38043 Grenoble, France
[c] CNRS, Laboratoire de Cristallographie, B.P. 166, 38042 Grenoble, cedex 9, France
[d] Laboratoire de Géophysique Interne et Tectonophysique, UMR CNRS/Université Joseph Fourier, 38400 Saint-Martin-D'Hères, France
[e] CEA/Grenoble, DRFMC/SP2M/NRS, 17 avenue des Martyrs, 38054 Grenoble, cedex 9, France

Abstract

X-ray absorption spectroscopy experiments were performed on a set of xenon implanted uranium dioxide samples. Results indicate that the gas forms highly pressurised inclusions as a result of temperature anneals or an external ion irradiation. Estimated bubble pressures were found to be in the region of 2–5 GPa at low temperature. The consequences of such high pressures developing within intra-granular bubbles in irradiated fuels are discussed. A model is given enabling the computation of the sink strengths of bubbles as a function of the pressure of the rare-gas they contain. The model predicts that for pressure values found in the experiments, fission gas bubbles do not act as sinks for diffusing rare-gas atoms.

PACS: 61.10.Ht; 64.75.+g; 66.30.Jt

1. Introduction

Following an irradiation in a commercial reactor, at least at burnups below 40 MW d kg^{-1}, equivalent to about four irradiation cycles, a great majority of the fission gases remain within the grains of the fuel. Fission gas release mechanisms have been studied extensively over many years through out-of-pile annealing experiments of fuels, usually sintered UO_2 pellets, base irradiated at relatively low temperatures (below ~1470 K). For fuels irradiated at burnups greater than 6 MW d kg^{-1} (e.g., [1–4]), fission gas release during a post-irradiation anneal occurs generally in three stages each involving several complex mechanisms. The first stage is characterised by rapid release also known as 'burst release' during which the release rate increases sharply over periods ranging from a few minutes to several tens of minutes; in the second stage release rates decrease and a diffusional regime begins to dominate; finally in the third stage, release levels off as trapping of migrating gas atoms becomes effective.

* Corresponding author. Tel.: +33 4 42 25 41 88; fax: +33 4 42 25 37 13.
E-mail address: garciap@drncad.cea.fr (P. Garcia).

0022-3115/$ - see front matter
doi:10.1016/j.jnucmat.2006.02.047

Modelling this release process, and especially its second stage, requires a description of the interaction between nanometre size intra-granular bubbles and diffusing gas atoms. If one assumes that intra-granular bubbles act as perfect sinks, then for fission gas bubble concentrations relevant to irradiated fuels, gas atoms homogenously distributed within the grain initially are readily trapped resulting in calculated gas release fractions [5] well below observed values. It would appear therefore that either intra-granular bubbles are imperfect sinks or that there exists a mechanism whereby gas may be transferred from within the grain to the grain boundary.

In this paper, an explanation is put forward as to why nanometre size bubble sink efficiencies may be lower than previously thought. In the first part, experimental evidence indicating the existence of highly pressurised fission gas bubbles is presented. This evidence is based on existing transmission electron microscopy (TEM) data relative to irradiated fuels. To complement this data, X-ray absorption spectroscopy (XAS) experiments were performed at the xenon K-edge of ion-implanted UO_2 samples. Following the low energy xenon ion implantation, samples were annealed at 870 K or ion irradiated. XAS is shown to provide an estimation of the gas pressures within the rare-gas atom inclusions. Finally, a simple model is proposed that enables the calculation of bubble sink efficiencies as a function of bubble characteristics. Its application to gas pressures derived from the XAS characterisation presented in the first part of the paper is discussed.

2. Evidence that intra-granular fission gas bubbles are pressurised

2.1. TEM data relative to irradiated fuels

Evidence of intra-granular bubbles, a few nanometres in size in irradiated UO_2 fuels has been reported for a wide range of burnups [6–8]. Observations point to a converging set of results in terms of bubble size distributions as estimated from TEM.

Kashibe et al. [7] examined samples at three different burnups (23, 44 and 83 MW d kg^{-1}). Observed specimens came from regions in the pellet that had experienced temperatures of around 1070 K. At the lowest burnup, bubble sizes and densities were found to be approximately 2 nm and $\sim 10^{24}$ m^{-3} respectively. At higher burn-ups, observations indicated a decrease in bubble population and a corresponding increase in bubble sizes (e.g., ~4 nm and 7×10^{23} m^{-3} at 44 MW d kg^{-1}), along with the emergence of bimodal bubble population, with larger bubbles in the 10–20 nm range.

Prior to these results, Thomas and Guenther [6] examined LWR fuel samples that had reached moderate burnups (30 MW d kg^{-1}) and had shown low gas release fractions (less than 1%). Observations revealed in samples taken from the outer part of the pellets the presence of fine scale intra-granular bubbles which ranged in size from 1 nm to about 10 nm. In the samples having operated at higher temperatures originating from a more central area of the pellet, the presence of larger bubbles apparently containing large quantities of xenon and krypton and associated with noble metal inclusions 50–100 nm in size. Energy Dispersive X-ray Spectroscopy (EDX) revealed that the density of the xenon–krypton phase in this central area was close to 2–3 g cm^{-3}. This would suggest the presence of noble gases in a highly pressurised form which was confirmed by the fact that the surrounding UO_2 matrix showed signs of being highly strained.

More recently, Nogita and Une [8] examined samples taken from the outer part of pellets irradiated to average burnups of 30, 44 and 83 MW d kg^{-1}. The TEM specimens examined revealed bubble sizes tended to increase as a function of burnup (~1 nm for the lower burnup to between 5 and 10 nm for the higher burnup specimens). Following Thomas' methodology, nano-EDX was successfully performed on 4–10 nm bubbles taken from the higher burnup samples and estimated xenon densities were in the 3.8–6 g cm^{-3} range. The upper values quoted by the authors would suggest solid xenon particles.

2.2. XAS analyses

To confirm these TEM results, XAS characterisations at the Xe K-edge (34561 eV) were performed of ion implanted samples. All the data were collected using a 13 element Ge fluorescence detector. The aim of these experiments was to determine the Xe local environment in the samples and its evolution upon a given treatment (temperature anneal or ion irradiation). If bubble formation occurred, by working at low enough temperatures, XAS results could be used to estimate Xe–Xe distances and coordination numbers, as has been done by other authors in different materials [9]. From a comparison with the cell parameter for fcc Xe (0.613 nm

at 5 K), one could then determine the xenon pressure within the aggregates. X-ray absorption near edge spectroscopy (XANES) and extended X-ray absorption fine structure (EXAFS) spectroscopy were carried out on the BM-08 (GILDA) and BM-30B (FAME) beam-lines at the European Synchrotron Radiation Facility (ESRF) in Grenoble. Because the Xe–Xe bonds are weak, data were generated at temperatures well below the xenon melting temperature (161.4 K) using a helium cryostat (i.e., at temperatures between 4 and 11 K).

Polycrystalline sintered UO_2 discs cut from dense UO_2 pellets were first polished and annealed at 1673 K for 4 h in a reducing atmosphere ($Ar + H_2$ 5%) so as to remove surface defects produced by the polishing process and insure the samples attained a stoichiometric composition. The samples were then implanted with xenon ions at the Institut de Physique Nucléaire de Lyon (IPNL). Doses and energies were chosen so that the xenon concentration reached a value of around 2 at.% over a distance extending approximately 150 nm from the sample surface.

The XAS results pertaining to four xenon ion implanted UO_2 samples are presented here: one as-implanted polycrystalline sample, two samples annealed at 870 K for 30 min and 12 h and one sample irradiated with 790 MeV Kr ions.

2.2.1. Effect of temperature anneals at 870 K

The normalised XANES spectrum collected at 5 K for the UO_2 sample annealed for 30 min at 870 K is compared in Fig. 1 to the spectrum calculated using the ab initio code FEFF8.20 [10] and the spectrum corresponding to the as-implanted sample. FEFF calculations have been performed with clusters of up to 45 atoms. However it appears that calculations involving 13 atom clusters reproduce the experimental XANES spectra and were therefore those we used in this study. This result corroborates previous studies (e.g., [11]) relative to krypton which showed that the first coordination shell only determined the near edge structure.

The resonance that appear in the spectrum relative to the annealed sample indicate that a discernable fraction of xenon atoms is not distributed randomly in the UO_2 matrix. Furthermore, the spectrum calculated using a cell parameter of 0.561 nm for solid xenon reproduces the experimental data indicating that the xenon aggregates present in the sample are in a solid, pressurised state. Further calculation results were obtained by modifying the cell parameter. These are indicated in Fig. 2 and show that an increase in cell parameter has the effect of shifting the XANES signal towards lower energies. The equation of state for solid xenon at around 0 K has been determined by Asaumi [12] who successfully fitted a Birch–Murnaghan type equation of state (EOS) to X-ray diffraction data. Using this equation of state, the cell parameter necessary to reproduce an experimental XANES spectrum was used to estimate the pressure within the solid xenon aggregates at 2.6 GPa. Based on the accuracy with which the position of a resonance in the XANES spectrum is determined, an estimation of the pressure in the aggregates using this method can only be done to within ±0.5 GPa.

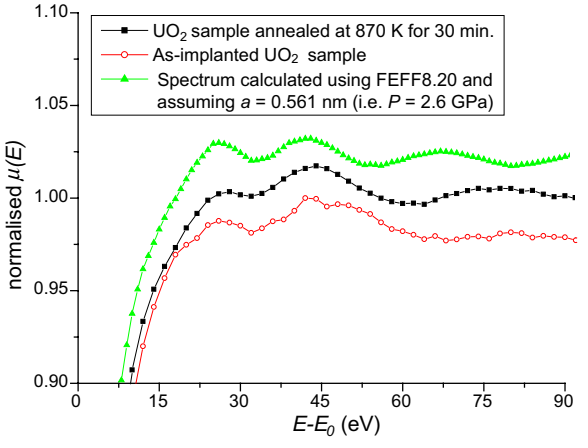

Fig. 1. Experimental XANES spectra of two Xe implanted UO_2 samples prior and after annealing, and comparison with a calculated XANES spectrum for Xe at 2.6 GPa.

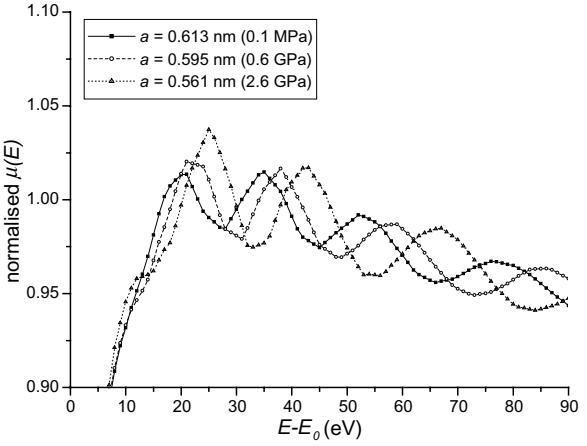

Fig. 2. Change in the XANES spectra as a function of the cell parameter hence pressure in xenon aggregates.

Whenever possible, EXAFS fits were also carried out to produce a more accurate estimation of Xe–Xe distances hence pressures within the aggregates. The experimental and calculated radial distribution functions at the xenon K-edge for UO_2 samples annealed at 870 K for 30 min and 12 h are given in Figs. 3 and 4. A second coordination shell clearly appears as a result of the longer anneal indicating longer range order around xenon atoms. The best-fit results including, Xe–Xe distances (R), coordination numbers (N) and Debye–Waller (σ^2) factors are given in Table 1 for both samples. The R_{factor} is an indicator of the quality of the fit. It is obtained from a least squares fit of the imaginary and real parts of the Fourier transform of the XAS oscillations. Xe–Xe distances are consistent with the presence of pressurised solid xenon inclusions in the sample. Using Asaumi's EOS [12] for solid xenon, the pressure within the aggregates can be estimated 2.7 ± 0.3 and 2.1 ± 0.3 GPa for the samples annealed for 30 min and 12 h respectively. This confirms the XANES estimation.

In an fcc crystal, one would expect 12 and 6 nearest neighbours for the first and second shells respectively. The values in Table 1 show that on average, each Xe atom contributing to the oscillations sees only about half the number of atoms expected. This is entirely consistent with the fact that the xenon atoms have precipitated to form nanometre size aggregates. A value of approximately 50% is theoretically expected for a 1 nm radius spherical inclusion.

2.2.2. *Effect of a high energy external ion irradiation*

A long presumed consequence of the passage of a fission fragment is the segregation of rare gas atoms

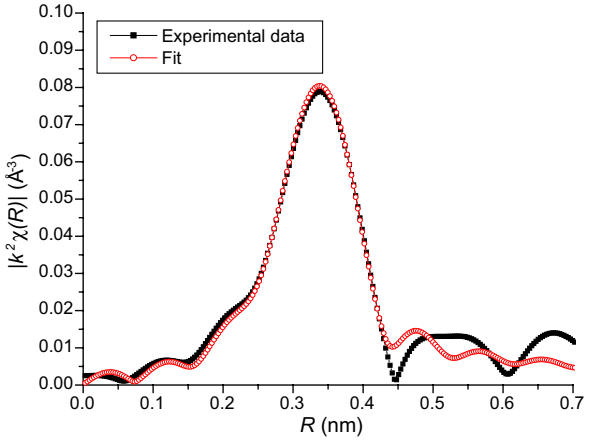

Fig. 3. Experimental and calculated Fourier transform moduli of the EXAFS signal obtained at the Xe K-edge for a Xe implanted UO_2 sample annealed at 870 K for 30 min.

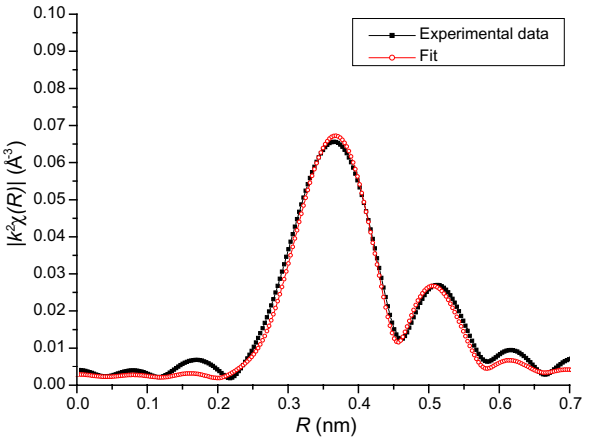

Fig. 4. Experimental and calculated Fourier transform moduli of the EXAFS signal obtained at the Xe K-edge for a Xe implanted UO_2 sample annealed at 870 K for 12 h.

Table 1
Results of the EXAFS fit for the annealed UO_2 samples

	Variables	Sample annealed at 870 K for 30 min	Sample annealed at 870 K for 12 h
First Xe–Xe coordination shell	N	6.1 ± 0.2	5.3 ± 0.4
	R (nm)	0.397 ± 0.002	0.404 ± 0.004
	σ^2 (nm^2)	$3 \times 10^{-4} \pm 10^{-4}$	$3.7 \times 10^{-4} \pm 2 \times 10^{-5}$
Second Xe–Xe coordination shell	N		2.3 ± 0.5
	R (nm)	–	0.532 ± 0.008
	σ^2 (nm^2)		$1.7 \times 10^{-4} \pm 4 \times 10^{-5}$
Fits are generally considered good when this parameter is less than 0.02	R_{factor}	0.006	0.018

Table 2
Extrapolation at 870 K of pressures estimated at low temperature

Sample treatment pressure (GPa)	Anneal at 870 K ~ 30 min	Anneal at 870 K 12 h	Irradiation with Kr ions to an ion dose of 10^{14} cm^{-2}
Estimated experimentally at ~5 K	2.7 ± 0.3	2.0 ± 0.3	4.7 ± 0.5
Extrapolated at 870 K	3.7 ± 0.3	3.0 ± 0.3	5.7 ± 0.5

lying in its wake [13]. This phenomenon, known as heterogeneous nucleation, has never been demonstrated explicitly but despite this, most in-pile fission gas behaviour models include it as a source term for nanometre bubble production. In order to ascertain whether this phenomenon is indeed relevant, a polycrystalline sample identical to those described above was irradiated with 790 MeV Kr ions to a dose of approximately 10^{14} cm^{-2}. The irradiation was performed at the Grand Accélérateur National d'Ions Lourds (GANIL) in Caen. The XAS methodology described above was then applied. An analysis of the XANES part of the spectrum indicated that xenon atoms had indeed segregated as a result of the ion irradiation into probably very small, highly pressurised inclusions. The pressure estimated at 5 K was around 4.7 ± 0.5 GPa. This is a clear indication that heterogeneous precipitation actually occurs i.e.: electronic excitation produced by the slowing of fission fragments is liable to cause rare gas precipitation.

Although no TEM results is yet available to complement the findings in terms of bubble size distributions, the results presented here confirm the experimental data obtained by Nogita et al. [8] pointing to the existence of highly pressurised rare gas aggregates. Our results would suggest a mechanism in which rare gas atoms cluster in the wake of fission fragments to form highly pressurised inclusions.

2.2.3. Extrapolation of estimated xenon pressures at 870 K

Because of its extreme relevance in-pile, the question arises as to the pressure and the state of the gas in the aggregates when they are formed i.e. at 870 K. A methodology was therefore developed which enables this estimation based on poro-elasticity theory. The EOS for xenon used at high temperature is that proposed by Casanova [14]. It is based on a Carnahan–Starling formulation which uses a modified Lennard–Jones potential. The UO_2 matrix is assumed to behave elastically. The results obtained of the extrapolation procedure are presented in Table 2 for all samples characterised. We examine in the following section the consequence on bubble sink efficiencies of such high pressures developing within xenon aggregates.

3. Modelling sink efficiencies of bubbles

In most fission gas release models, the kinetic term relative to the capture by bubbles of migrating rare gas atoms, otherwise known as sink efficiency of bubbles is determined by assuming that bubbles act as perfects sinks [15]. More important though, the stress distribution around the bubble is neglected when deriving the sink efficiency. In this case, the rate of capture S_b by a gas bubble of mobile atoms is expressed as:

$$S_b = 4\pi R_b D_{xe} C_{xe}, \tag{1}$$

where R_b is the bubble radius, C_{xe} the intra-granular gas concentration away from the gas bubble and D_{xe} is the xenon volume diffusion coefficient. This term is obtained by assuming that a steady state gas concentration is reached rapidly around the bubble and therefore, by solving the time independent diffusion equation in spherical coordinates, with boundary conditions such that the gas concentration at the bubble surface is zero and at infinity C_{xe}. We now examine the possible effect of very high pressures developing within the bubble.

3.1. Model development

Because intra-granular bubbles are spherical, it is assumed that the stress distribution around them presents a spherical symmetry. If the bubble is highly pressurised, then the radial stress at the bubble–matrix interface will be highly compressive. It can be shown [15] that the internal energy variation of a system for which the stress tensor presents a spherical symmetry characterised by the stress vector (σ_{rr}, $\sigma_{\theta\theta}$, $\sigma_{\phi\phi}$) corresponding to the introduction of a chemical or quasi-chemical species (such as a vacancy) is:

$$\Delta E = \sigma_{rr} \Delta V_{\alpha}, \tag{2}$$

where ΔV_α is the volume change of the system due to the introduction of an extra atom, or vacancy as the case may be.

Applying relation (2) to the expression of the chemical potential μ_α of a species α yields:

$$\mu_\alpha = k_b \cdot T \cdot \ln(C_\alpha) - \Delta V_\alpha \sigma_{rr}, \tag{3}$$

where k_b is Boltzman's constant, T the temperature.

Let $\vec{\nabla}\sigma_{rr}$ be the radial stress gradient around the bubble. The flux of particles J_α in a region around the bubble can be expressed using expression (3) for μ_α as:

$$\begin{aligned} J_\alpha &= -L_\alpha\left(\vec{\nabla}\mu_\alpha\right) \\ &= -L_\alpha\left(k_b T\frac{\vec{\nabla}C_\alpha}{C_\alpha} - \Delta V_\alpha \vec{\nabla}\sigma_{rr}\right) \\ &= -D_\alpha\left(\vec{\nabla}C_\alpha - \frac{C_\alpha \Delta V_\alpha}{k_b T}\vec{\nabla}\sigma_{rr}\right). \end{aligned} \tag{4}$$

Eq. (4) is only a variation on a theme developed by other authors relative to stress induced diffusion of point defects around dislocations (see [16,17] for instance). It shows that the stress gradient around the bubble is a thermodynamic force in the same way as the concentration gradient. If a bubble is highly pressurised, then the stress gradient is positive and the flux of gas atoms will be reduced with respect to an analysis in which the stress gradient is not taken into account.

$\vec{\nabla}\sigma_{rr}$ can be established assuming the existence of an elastic stress field around the bubble and that the radial stress at the bubble–matrix interface and at infinity from the bubble centre are given by the following expressions respectively:

$$\sigma_{rr}(R_b) = -P_b + \frac{2\gamma}{R_b}, \quad \sigma_{rr}(\infty) = \sigma_h, \tag{5}$$

where P_b is the internal bubble pressure, γ the bubble–matrix interfacial tension and σ_h the fuel hydrostatic stress at what can be considered as infinity from the centre of the bubble.

With boundary conditions (5), $\vec{\nabla}\sigma_{rr}$ is given by:

$$\vec{\nabla}\sigma_{rr}(r)\cdot\vec{u}_r = \frac{d\sigma_{rr}}{dr} = \frac{-3R_b^3}{r^4}\left(-P_b - \sigma_h + \frac{2\gamma}{R_b}\right). \tag{6}$$

In Eq. (6), $\vec{u}_r$ is the unit normal vector at distance r from the bubble centre.

Assuming a steady state situation is reached, conservation of species a is given by:

$$\nabla \cdot \vec{J}_\alpha = 0. \tag{7}$$

Also assumed, following [18], is the expression for the diffusion coefficient D_α as a function of the radial component of stress:

$$D_\alpha = D_\alpha(\sigma_{rr} = 0)\cdot e^{\frac{\sigma_{rr}(r)\Delta V_\alpha}{k_b T}}. \tag{8}$$

The above expression assumes that the diffusion coefficient is proportional to the vacancy concentration in the material and that this concentration is reduced due to the local compressive radial stresses around the bubble.

Now substituting (8) and (6) into (4) and the resulting relationship into (7) yields the differential Eq. (9) that governs the change in concentration C_α at a distance r from the bubble centre:

$$\frac{d^2}{dr^2}(C_\alpha) + \frac{2}{r}\frac{dC_\alpha}{dr} - \left(\frac{6f}{r^5} + \frac{9f^2}{r^8}\right)C_\alpha = 0, \tag{9}$$

where f can be expressed as follows:

$$f = R_b^3\left(-P_b - \sigma_h + \frac{2\gamma}{R_b}\right)\frac{\Delta V_\alpha}{k_b T}. \tag{10}$$

In the following paragraph, the sink efficiency of a bubble when its inner gas pressure is taken into account is compared to expression (1).

3.2. Discussion

Eq. (9) was solved numerically for two temperatures, 870 and 1670 K using the boundary conditions $C_\alpha(R_b) = 0, C_\alpha(\infty) = 1$ for two bubble radii: 1 nm and 5 nm. The flux of species α at the bubble surface was then evaluated from which the stress dependent rate of capture of gas atoms by the bubble S'_b could be calculated. Fig. 5 shows the ratio S'_b/S_b for both temperatures and for small and larger bubble sizes. It clearly points to the sink efficiency being greatly reduced for bubble pressures greater than 3.5 GPa, irrespective of pressure or size. At 870 K, for bubble pressures corresponding to those presented in Table 2, the sink efficiency of a 2 nm size bubble is virtually zero. This brings us round to making a few important comments. Firstly, it would appear that resolution parameters used in fission gas release models to strike a balance between gas atoms in bubbles and randomly dispersed in the fuel matrix should be reassessed. Our results clearly shed light on the important difficulty in justifying, based on known physical processes, the high values usually used for the gas resolution parameters. Furthermore it is now reasonable to assume, that under steady state irradiation conditions,

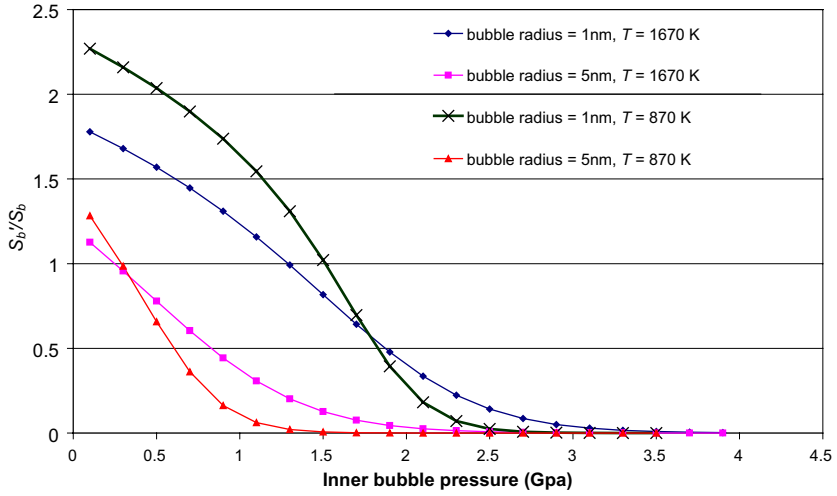

Fig. 5. S'_b/S_b as a function of internal bubble pressure.

fission gas atom resolution should be viewed in terms of wholesale destruction of bubbles as opposed to the resolution of individual gas atoms.

At 1670 K, the bubble pressure at which the sink efficiency reaches values closer to those previously assumed is shifted towards lower pressure values. Our results would explain why trapping by bubbles is initially inhibited during annealing experiments of irradiated fuels. The time at which trapping effects begin to dominate again (third release stage referred to in the previous section) can be interpreted as the time it takes for vacancies to flow to the bubbles. This phenomenon induces bubble growth and a decrease in the bubble inner gas pressure.

The model presented here is not restricted to application to fission gas atoms. It can also be applied to vacancies simply by changing the sign and value of ΔV_α. Such an application has shown that the sink efficiency of 5 nm bubbles with respect to vacancies increases by less than a factor of three at very high pressures. This implies that for annealing experiments, the application of our model should not fundamentally change the currently predicted bubble growth kinetics.

4. Conclusions

XAS has been applied to the characterisation of xenon bubbles in ion-implanted UO_2 samples. The results indicate that rare-gas bubbles that appear as a result of temperature anneals at 870 K or external ion irradiations are highly pressurised. The results strongly point to electronic excitation produced in irradiated material by slowing fission fragments being responsible for fission gas atom segregation in UO_2 into highly pressurised bubbles. The number of nearest neighbours which was found to be approximately half that expected indicates the presence of small clusters, approximately 2 nm in size. On-going TEM work should confirm the presumed size of the aggregates. Gas pressures estimated at low temperature were further extrapolated at higher temperatures. It has thus been demonstrated that XAS is ideally suited for characterising rare gas atom aggregates in UO_2 with no prior assumption as to aggregate geometry.

A simple model which enables the computation of bubble sink efficiencies has been derived which contrary to previous models is a function of pressure within the xenon aggregates. It has thus been demonstrated that at pressures estimated from the XAS characterisation, small size bubble sink efficiencies are virtually zero. If confirmed, this has important consequences for our understanding of in-pile and out-of-pile fission gas release. As regards out-of-pile annealing experiments, our results suggest that it is the high pressures within the aggregates that explain the apparently volume diffusion controlled release stage generally observed. Regarding in-pile release, it appears that the implementation of our model in a fission gas behaviour model would result in the reassessment of the fission gas re-solution parameter, in line with values expected from known physical processes.

Acknowledgements

The authors wish to express their extreme gratitude to the accelerator team of the IPNL and to C. Peaucelle in particular, for carrying out the ion implantations of the samples presented in this study. Are also sincerely acknowledged the contributions of N. Benyagoub and S. Bouffard at the GANIL in Caen, where the high energy ion irradiations referred to here were performed.

This paper is dedicated to the memory of Thierry Petit who tragically left us just over three years ago. Since then, his colleagues have tried to follow in a track that he had traced. More than his guidance though it is his friendship and kindness that are most sorely missed.

References

[1] C. Baker, J.C. Killeen, Materials for Nuclear Reactor Core Applications, BNES, London, 1987, 153.
[2] K. Une, S. Kashibe, J. Nucl. Sci. Technol. 27 (1990) 1002.
[3] I. Zacharie, PhD Thesis DMT/SEMI CEA Saclay, 1997.
[4] S. Valin, PhD Thesis, DTP/SECC CEA Grenoble, 1999.
[5] R.J. White, in: Proceedings of IAEA Technical Committee Meeting, June 2000, Winderemere, UK.
[6] L.E. Thomas, R.J. Guenther, Mater. Res. Soc. Symp. Proc. 127 (1989).
[7] S. Kashibe, K. Une, K. Nogita, J. Nucl. Mater. 206 (1993) 22.
[8] K. Nogita, K. Une, Nucl. Instrum. and Meth. B 141 (1998) 481.
[9] G. Faraci, A.R. Pennisi, A. Terrasi, S. Mobilio, Phys. Rev. B 38 (1988) 13468.
[10] M. Newville, J. Synch. Rad. 8 (2001) 322.
[11] A. Di Cicco, A. Filipponi, J.P. Itié, A. Polian, Phys. Rev. B 54 (1996) 9086.
[12] K. Asaumi, Phys. Rev. B 29 (1984) 7026.
[13] J.A. Turnbull, J. Nucl. Mater. 38 (1971) 203.
[14] E. Casanova, PhD Thesis, Université d'Aix-Marseille I, March 1998.
[15] D.R. Olander, Fundamental aspects of nuclear reactor fuel elements, energy research and development administration, 1976.
[16] W.G. Wolfer, M. Ashkin, J. Appl. Phys. 46 (1975) 547.
[17] N. Smetniansky-De Grande, E.J. Savino, C.N. Tomé, Phys. Stat. Sol. (b) 144 (1987) 271.
[18] M.J. Aziz, in: Proceedings of International Conference on Simulation of Semiconductor Processes and Devices, Cambridge MA, September 2003.